Journal of Applied Research and Technology

www.jart.icat.unam.mx

Journal of Applied Research and Technology 23 (2025) 371-380

Original

Portable mini antenna for detecting and distinguishing between types of hemorrhagic stroke

J. N. Shehab[a,b]* M. J. Farhan[a] S. Al-Azawi[b]

[a]*University of Mustansiriyah, Baghdad, Iraq*
[b]*University of Diyala, Diyala, Iraq*

Received 09 17 2024; accepted 11 22 2024
Available 08 31 2025

Abstract: Stroke is a major cause of disability and death worldwide, and it constitutes a considerable burden on global health. Thus, prompt detection of strokes reduces the possible risk of death. In this work, an antenna in the form of a Moroccan decoration was proposed for early detection of hemorrhagic stroke. This includes testing the five main types of hemorrhagic stroke, which are subdural, epidural, subarachnoid, intracerebral, and intraventricular, and this method provides the possibility of distinguishing between them, thus reducing the rate of death and disability by a large percentage. The proposed antenna is characterized by its small size with dimensions of 30×35×0.62 mm3, a resonance frequency of 2.806 GHz, a 3.196 GHz bandwidth, and a 2.8 dB gain. The simulation results of the proposed antenna show high efficiency in detecting and distinguishing hemorrhagic strokes, as indicated by clear changes in resonance frequency and return losses S11 caused by brain percentage change due to hemorrhagic stroke.

Keywords: Hemorrhagic stroke, RF sensor, detection of stroke, types of hemorrhagic strokes, wearable antenna.

*Corresponding author.
E-mail address: jinan-alazawii@uomustansiriyah.edu.iq (J. N. Shehab).
Peer Review under the responsibility of Universidad Nacional Autónoma de México.

1. Introduction

A stroke is the interruption of the blood supply carrying oxygen and nutrients to critical areas of the brain. Such an interruption leads to the loss of cell' function, which in turn causes disability or even death for the patient. (Liu et al., 2023). Stroke kills 5 million people each year and leaves others permanently damaged. It is the third leading cause of death after heart disease and cancer, and the second leading cause of disability worldwide. Therefore, rapid and accurate diagnosis and monitoring of treatment can reduce such risks. (Tobon Vasquez et al., 2022).

Stroke is divided into two types: hemorrhagic and ischemic. Ischemic stroke occurs due to an interruption of blood supply within a blood vessel, caused by the formation of a blood clot inside the blood vessel. In contrast, hemorrhagic stroke occurs when a blood vessel in the brain bursts, causing blood to accumulate and press on the surrounding brain tissue. Hemorrhagic strokes are divided into epidural, subdural, subarachnoid, intracerebral, and intraventricular. These types differ in the size, shape, and location of the bleeding area within the skull, but the symptoms are similar in all types. These symptoms include sudden severe headache, dizziness, loss of balance, nausea, and vomiting. Misdiagnosis and delay of stroke may lead to the prescription of inappropriate medication, which may cause death or permanent disability. (Phan et al., 2018; Sohani et al., 2019).

The consequences of delaying stroke diagnosis cause a loss of 1.9 million neurons, 14 billion synapses, and twelve kilometers of myelinated white matter every minute, hence the principle that “time is of the essence for the brain” arose. Furthermore, it is worth noting that 40% of cases result in death before reaching the hospital. So, it is important to reduce the time required to diagnose the type of stroke to prescribe suitable care. (Alon & Dehkharghani, 2021). Thus, various papers have been published to provide fast and accurate methods for early stroke detection.

Salleh et al. (2019) proposed nine antipodal Vivaldi antennas for stroke detection. The proposed antennas operate from 2.06 to 2.61 GHz with a 550 MHz bandwidth dimensions of 60×50×1.524 mm^3 and a gain of 2.45 dB. Smida and Smida (2020) proposed using five antennas with different designs to detect and locate the stroke based on the SAR. Four antennas have dimensions of 66×66 mm^2, and the fifth antenna, which is recognized as the most efficient among them, has dimensions of 40×66 mm^2. The test configuration was in the form of an array consisting of eight antennas at a time, and all of them worked at a resonance frequency of 2.4 GHz. Naghavi et al. (2023) designed a bowtie patch antenna based on UWB microwave radars to detect strokes and bleeding areas inside the head. The proposed antenna targeted the unexpected stroke shapes, specifically. The reflected signal is converted to an image to determine the location of the stroke. This was done by placing 16 antennas around the head, each with dimensions of 25×25×2 mm^3 and (1.2-4.5) GHz bandwidth, but the SAR was not calculated. Anwar et al. (2024) used five crescent-shaped sensors of different sizes and efficiencies to detect brain atrophy and stroke. One sensor with glasses was fixed on each side of the head to ensure continuous patient monitoring. Three different locations were used to detect hemorrhagic stroke, but the type of stroke was not specified. Singh et al. (2024) used two antennas placed side by side above the head to detect brain hemorrhage. Machine learning was combined with microwave sensors to obtain high accuracy in diagnosing the presence of a brain hemorrhage. The resonance frequency was 2.45 GHz, (1.5-3.17) GHz bandwidth, and the radius dimensions were 33×33× 0.8 mm^3.

The lack of rapid response or misdiagnosis plays a critical role in the stroke effect. Therefore, the development of medical engineering led to more research being published to introduce devices for detecting the stroke type and its progression stage. Such devices ensure that they are: low-cost, small, wearable, portable, highly flexible, and have accurate results. Thus, to achieve this, microwave imaging technology was introduced as an effective solution in neurological medical applications, especially in detecting abnormal tissues. It provides a way to detect the disease and determine its type before the patient reaches the hospital. It can be easily placed in ambulances, which increases the chances of prescribing the proper treatment quickly and reducing damage to the brain. Thus, in this work, a small, portable, and highly efficient antenna was designed and tested to detect and recognize the five main types of hemorrhagic stroke. The proposed antenna has dimensions (30 × 35 × 0.62) mm^3 and a bandwidth of (2.53-5.726) GHz. While the resonance frequency is less than 3 GHz.

The rest of this paper is organized as follows: Section 2 introduces the antenna design steps. Section 3 includes the phantom model head, and in Section 4, the simulation results are discussed. The sensor action in hemorrhagic stroke is listed in Section 5. The Specific Absorption Rate (SAR) is presented in Section 6. In Section 7, the analysis and comparison results are discussed. Finally, conclusions are drawn in Section 8.

2. Antenna design steps

In this section, the initial design of the proposed antenna with a Moroccan decoration shape is introduced. The antenna size is (30 × 35 × 0.62) mm^3 and has a bandwidth of (2.53-5.726) GHz. The antenna ground and patch are made from annealed copper, and the substrate is FR4 material. The dielectric constant of the substrate is 4.3, the loss tangent is 0.02, and

the dielectric constant for the patch and ground is 0.035. The antenna design steps and parameters are shown in Fig. 1 and Table 1. The initial dimensions of the antenna are determined as follows (Samsuzzaman et al., 2023):

$$W = \frac{c}{2f_r}\sqrt{\frac{2}{\varepsilon_{r+1}}} \quad (1)$$

$$\varepsilon_{reff} = \frac{\varepsilon_r+1}{2} + \frac{\varepsilon_r-1}{2}\left(1+12\frac{h_s}{w}\right)^{-\frac{1}{2}} \quad (2)$$

$$L = \frac{c}{2\,f_r\sqrt{\varepsilon_{reff}}} \quad (3)$$

Where: W is the width of the patch, c is the vacuum light speed, f_r refers to the resonant frequency, ε_r refers to the relative dielectric permittivity, ε_{reff} is the effective permittivity of the substrate, h_s is the thickness of the substrate patch. L is the length of the patch.

After finding the initial dimensions to achieve the required frequency, the rectangular-shaped patch was formed into nine connected circles as shown in step 2 in Fig. 1(a). The shape was merged with nine circles of the same size and details, but with rotation angles of 30 ° and 60 ° to resemble Moroccan decorations, as depicted in step-3 Fig. 1(a), (c). The ground is cut and adjusted to achieve UWB with good directivity and gain, as shown in step 4 in Fig. 1 (a).

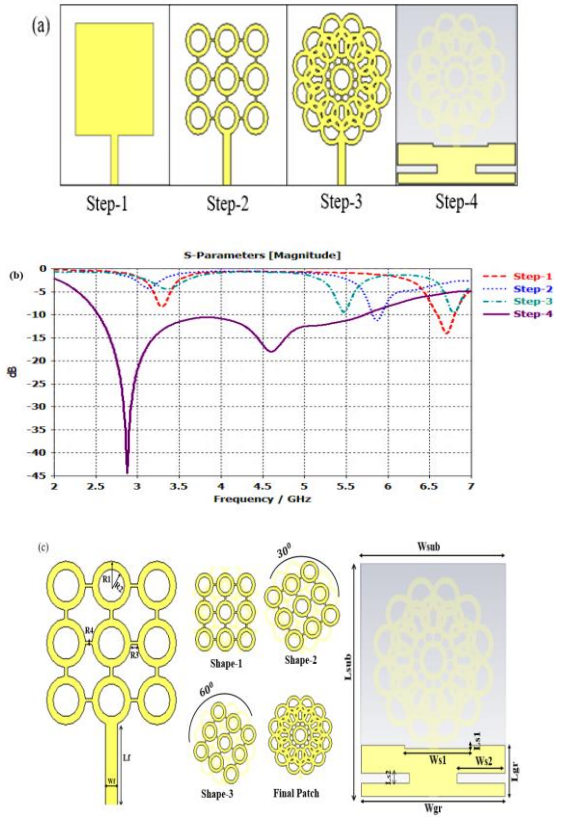

Figure 1. (a) Steps of the proposed antenna design, (b) S11 for each step, and (c) parameters of the proposed antenna shape.

Table 1. Parameters of the proposed sensor model.

Parameter	Description	Dim. (mm)
R_1	The radius of the outer circle	3
R_2	The radius of the inner circle	2
R_3	Length of bridge between two circles	1
R_4	Width of bridge between two circles	0.4
W_f	Width of feedline	1.9
L_f	Length of feedline	10.7
L_{sub}	Substrate length	35
W_{sub}	Substrate width	30
L_{gr}	Ground length	7.8
W_{gr}	Ground width	30
Ls1	Length of the slot in the ground	0.5
Ws1	The width of the slot in the ground	14
Ls2	length of slot-2 in the ground	1.5
Ws2	Width of the slot-2 in the ground	10
h_s	The thickness of the substrate patch	0.62

3. The Phantom head model

Computer Simulation Technology Studio (CST) 2023 was used to create and simulate the human head model. The head model consists of seven layers, which include: skin, fat, skull, dura, cerebrospinal fluid (CSF), gray matter, and finally white matter, with different dielectric properties for each layer. (Lalitha & Manjula, 2024). The parameters of the head model are listed in Fig. 2 and Table 2.

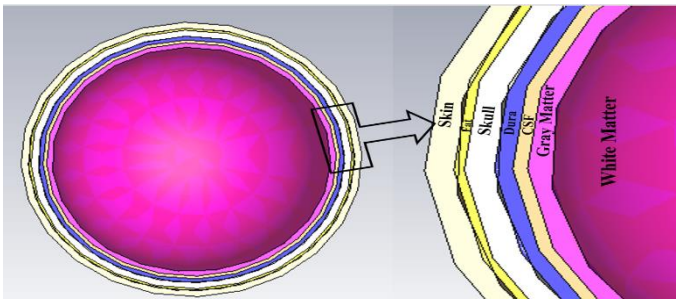

Figure 2. Head phantom layers proposed format by CST program.

Table 2. Parameter values of the head phantom at 2.878 GHz resonance. (*Https://Itis.Swiss/Virtual-Population/Tissue-Properties/Database/Database-Summary/*, n.d.)

Tissue	ε_r (F/m)	σ (S/m)	ρ (kg/ m^3)	Thickness (radius) (mm)
Blood	57.6	2.93	1050	-
White matter	35.7	1.44	1041	81
Gray matter	48.2	2.12	1045	82
Cerebrospinal fluid (CSF)	65.6	3.88	1007	83
Dura	41.5	1.93	1174	83.5
Skull	11.1	0.481	1908	87.6
Fat	10.7	0.327	911	89
Skin	37.6	1.68	1109	90

4. Results and discussion

4.1. Reflection characteristic

The effectiveness of using sensors in neurodiagnostic applications must be evaluated. Thus, the first test was the reflectance measurement (S11) (Anwar et al., 2024). The computational analysis was performed using the sensor in the free space, and then the measurements were made near the tissues, as shown in Fig. 3.

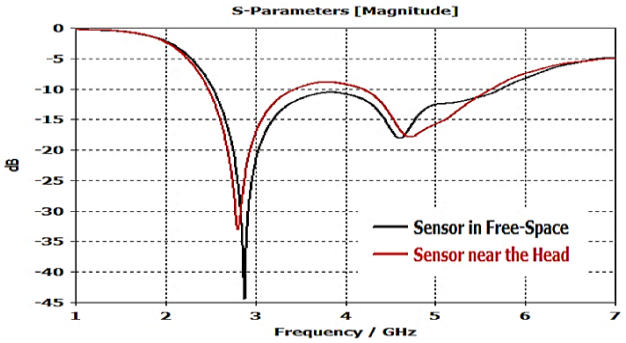

Figure 3. Comparison of reflection loss (S11) between Free Space and Near field of the head.

From Fig. 3, it is evident that the sensor has two resonant frequencies: 2.878 GHz and 4.6059 GHz, which are suitable for neurodiagnostic applications. (Anwar et al., 2024). The first frequency is less than 3 GHz, and therefore, it is suitable for penetrating the middle of the white matter. While the second is suitable for penetrating the gray matter. In addition, the bandwidth of 3.1926 GHz is suitable for converting the reflected signal into an image to detect the location and size of the brain hemorrhage. (Singh et al., 2024).

4.2. The Gain and the voltage standing wave ratio (VSWR)

Small antennas are preferred in contemporary neurodiagnostic applications because of their ease of transport and usage. This is a problem because of directivity and gain decrease with antenna size. However, the proposed small antenna provides good gain and directivity and a VSWR value of less than 2. Thus 90% of the source power is transferred to the antenna, as illustrated in Fig.4 and Table 3. In addition to the above tests, the Front-to-Back Ratio (FBR) was evaluated. The FBR represents the ratio of radiated power in the front-to-back direction. (Anwar et al., 2024). The higher the FBR, the better the antenna efficiency and directivity suitable for neurological medical diagnosis, as stated in Table 3.

Table 3. Values of gain, directivity, FBR, and VSWR for the proposed sensor.

Antenna location	f_r (GHz)	Gain (dB)	Directivity (dBi)	VSWR	FBR (dB)
Free-space	2.878	1.92	2.46	1.012	0.605
	4.6059	1.06	2.96	1.28	3.38
Health brain	2.806	3.58	6.1	1.046	18.26
	4.732	3.39	5.15	1.24	19.6

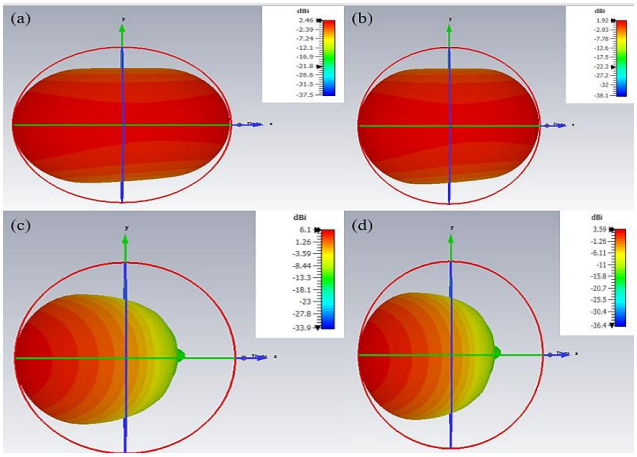

Figure 4. Directivity (a) in free space and (c) near the head phantom and gain (b) in free space and (d) near the head phantom.

4.3. Radiation pattern

The far-field radiation pattern of the antenna shows the direction of the power being transmitted in the forward direction, with a decrease in the backward direction. Thus, it represents an important metric to evaluate the performance of the proposed antenna. (Alqadami et al., 2021).

As depicted in Fig.5, it is clear that the antenna's radiation pattern is symmetrical in free space, with the major lobe orientation at 16.7 dB and 15.8 dB at 2.878 GHz and 4.6059 GHz, respectively. The semi-directional radiation has a main lobe direction of 18.4 dB and a side lobe of -18 dB at 2.806 GHz and 18.1 dB with the side lobe of -8 dB at 4.732 GHz when the head model is utilized.

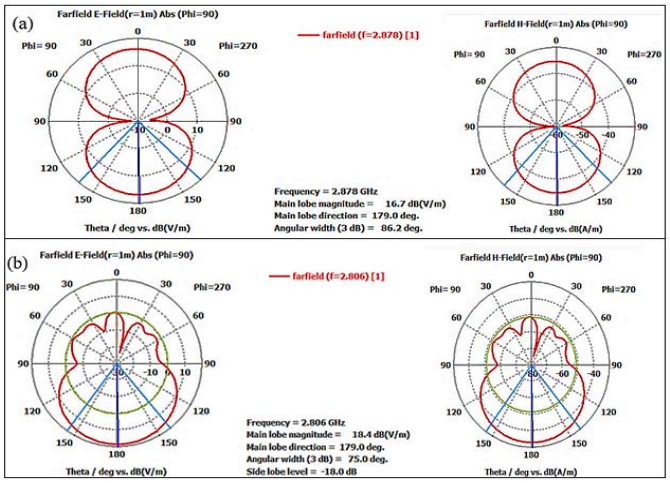

Figure 5. Radiation pattern (a) sensor in free space, (b) sensor near the head phantom.

4.4. Surface current and current density

To understand the efficiency of the antenna, it is necessary to know the path of the current and the important flow points between the feeding point, the radiating patch, and the ground. (Alqadami et al., 2021). It is possible to notice the openings in the radiating patch and the ground, which increase the density of the current at those points.

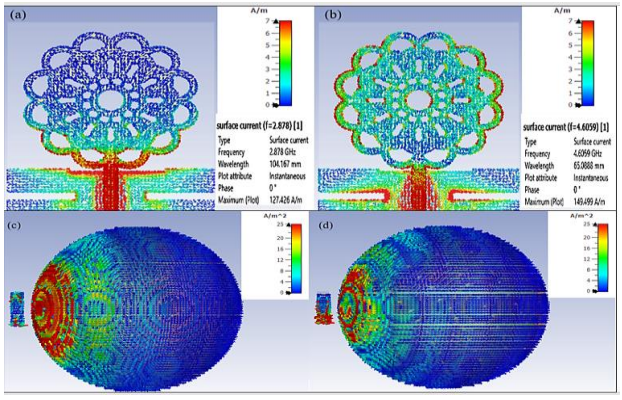

Figure 6. (a) and (b), surface current in free space; (c) and (d), current density near the head phantom for the sensor.

From Fig. 6 (a) and 6(b), it is evident that the distribution of the current at 2.878 GHz is mainly produced from the letter U of the sensor ground, feedline, and the outer edges of the radiating patch. This area caused the frequency to be less than 3 GHz, while the 4.6 GHz frequency is concentrated at the side slots of the sensor ground, in addition to the feedline. Fig. 6 (c) and 6(d) show the current distribution density near the head.

5. Sensor action in hemorrhagic stroke

5.1. Epidural hemorrhage

It is the bleeding between the inner part of the skull and the outer cover of the brain, which is called dura mater. It occurs due to a blood vessel, often an artery, rupturing because of skull fractures. Such bleeding causes blood to collect, forming a hematoma. The larger the size of this hematoma, the more pressure there is on the brain, and the bleeding spreads around the outer cover of the brain (Zohor et al., 2024). As blood has a higher dielectric constant, the permittivity of white and gray matter is increased by up to 20%. Such an increment in white and grey matter provides the possibility of detecting, identifying, and classifying the stroke (Liu et al., 2023), as shown in Fig. 7 and Table 4.

Table 4. The change in the dielectric properties of white and gray matter in hemorrhagic stroke.

Tissue	10% increase for 5 mm stroke hematoma		20% increase for 10- and 20-mm stroke hematoma	
	ε_r (F/m)	σ (S/m)	ε_r (F/m)	σ (S/m)
White matter	39.27	2.12	42.84	2.12
Gray matter	53.02	2.12	57.8	2.12
Stroke hematoma	63.36	3.22	69.12	3.516

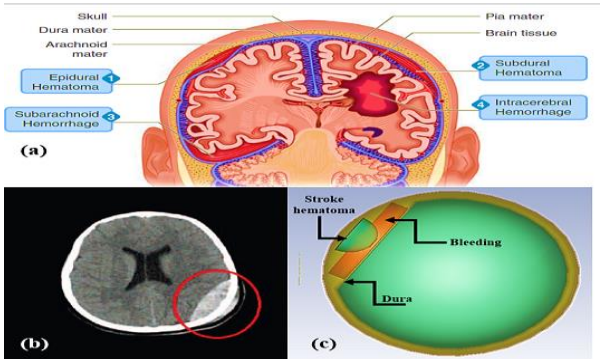

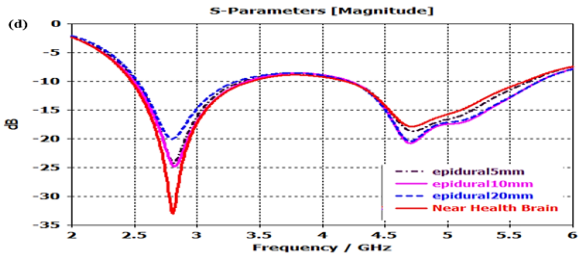

Figure 7. (a) Types of hemorrhagic strokes in the brain (IsHak, 2023), (b) A CT scan of epidural hemorrhage (Phan et al., 2018), (c) proposed format by CST program, and. (d) comparison of S11 of three different sizes (5,10,20) mm of epidural stroke.

According to Figure 7(d), it is possible to observe that the sensor differentiates between hemorrhagic clusters based on size and the difference in electrical characteristics with increasing size. However, they are the same type of hemorrhagic stroke, thus giving the paramedic the possibility of knowing the damage that occurred to the brain and prescribing the exact treatment based on the accuracy of the detection.

5.2. Subdural hemorrhage

It is a rupture of the pontine veins that represent the junctions between brain cells. It leads to bleeding between the inner edge of the dura mater and the arachnoid membrane. It is the most common condition associated with head trauma resulting from abuse. It can be noticed that, similar to epidural bleeding, it appears as a convex shape that presses on the brain, forming a thick layer of blood (Geoghegan et al., 2023), as depicted in Fig. 8.

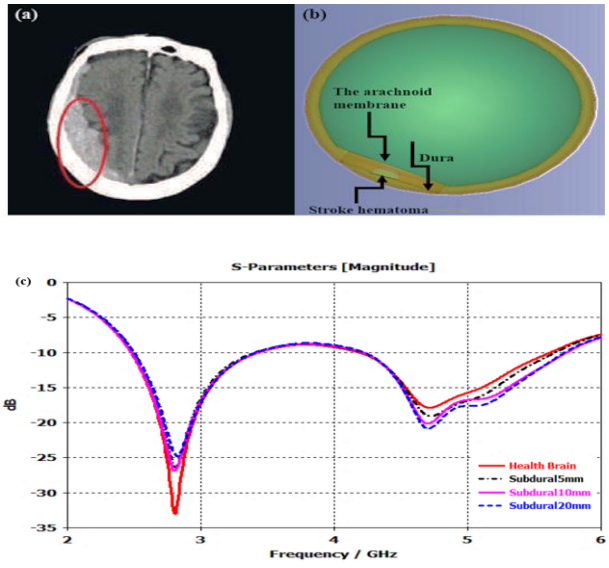

Figure 8. (a) A CT scan of a subdural hemorrhage (Phan et al., 2018), (b) proposed format by CST program, and (c) comparison of S11 of three different sizes (5,10,20) mm of subdural stroke.

Through the result in Fig. 8 (c), it is possible to observe the accuracy of the sensor in differentiating between different sizes of the same type of subdural hemorrhagic stroke.

5.3. Subarachnoid hemorrhagic

This type of bleeding is a global health burden with high rates of mortality and permanent disability. It results from the rupture of blood vessels within the skull, the leakage of blood into the inner space (pia mater) and the middle layer (arachnoid), and the mixing of blood with cerebrospinal fluid. It occurs due to sudden high blood pressure, emotional shock, sudden exercise, and alcoholism (Dreier et al., 2024). The simulation results are shown in Fig. 9.

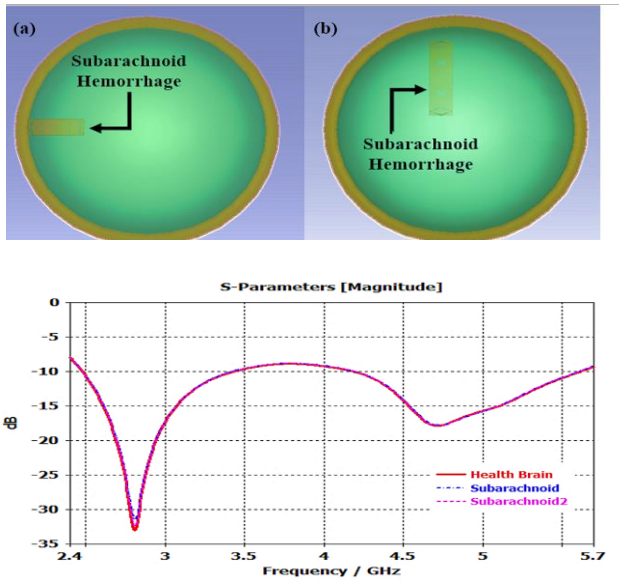

Figure 9. (a) and (b), proposed format by CST program, and (d) comparison of S11 in two different places for subarachnoid hemorrhage with a size of 20mm.

5.4. Intracerebral hemorrhage

It is a devastating type of stroke where a hematoma forms inside the brain tissue due to the rupture of one of the blood vessels feeding the brain. This leads to blood leaking into the brain tissue and the brain membranes, which causes a cut-off of the brain's perfusion. If the brain is cut off for more than 4 to 6 minutes, the brain tissue dies and loses its function. It occurs due to high blood pressure, protein accumulation inside the artery walls, and the use of anticoagulant medications (Karunarathna et al., 2024), as shown in Fig. 10 (a) and 10(d).

5.5. Intraventricular hemorrhage

It is bleeding that occurs in the ventricular system of the brain, where the cerebrospinal fluid is produced. This condition is common in infants, especially those born prematurely or with a weight lower than usual. This type is classified into primary

and secondary. The primary is limited to the ventricular system, accounting for 30%. The secondary type occurs when bleeding extends within the brain tissue under the arachnoid, representing approximately 70%. Other causes of this type include head trauma and malformation of the blood vessels within the brain (Essibayi et al., 2023). The results of the primary and secondary intraventricular hemorrhage are shown in Fig. 10 (b) and 10(c).

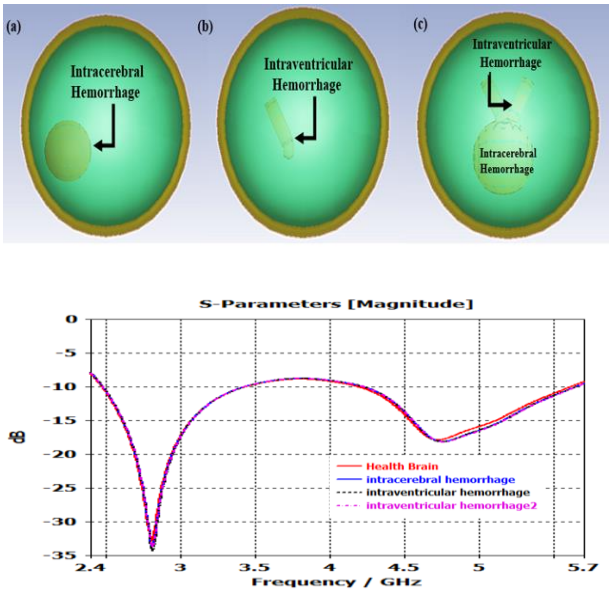

Figure 10. (a), (b), and (c), proposed format by CST program for intracerebral, primary, and secondary intraventricular; and (d) comparison of S11 for intracerebral, primary, and secondary intraventricular with a size of 20 mm.

6. Specific Absorption Rate (SAR)

The safety requirements of tissues when exposed to electromagnetic waves were set by the Federal Communications Commission (FCC) and the International Commission on Non-Ionizing Radiation Protection (ICNIRP). Thus, SAR must be considered in the design of communication and wearable devices so that it does not exceed the permissible safety limits (Abdul-Al et al., 2022). The SAR should not exceed 1.6 W/kg and 2 W/kg for tissue masses weighing 1 and 10 grams. The SAR values were calculated using an input power of 100 mW, as shown in Fig. 11 and Table 5. It was evident from both Fig. 11 and Table 5 that the SAR value is within the safe level.

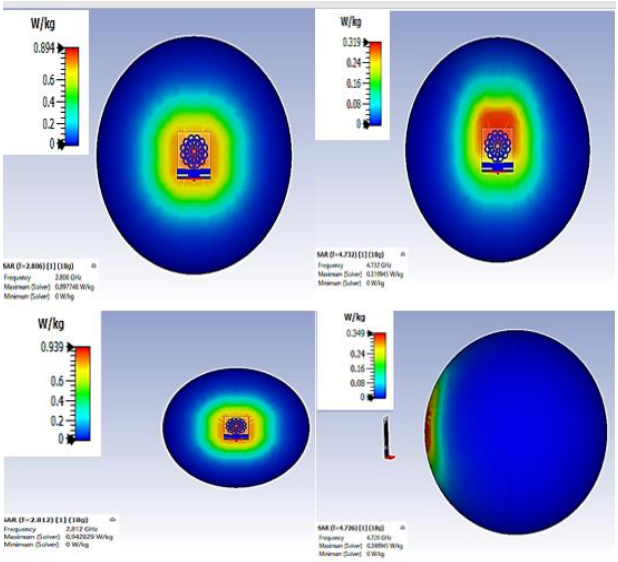

Figure 11. SAR at the resonance frequency for healthy brain and stroke.

Table 5. Shifting in resonance frequency, return loss, and the SAR.

Brain State	f (GHz)	Δf (MHz)	$S11$ (dB)	$\Delta S11$ (Db)	SAR (W/Kg)
Healthy	2.806	-	-33	-	0.894
	4.732	-	-17.8	-	0.319
Epidural-5 mm	2.812	6.1	-24.1	8.86	0.844
	4.726	6	-18.6	0.82	0.493
Epidural-10 mm	2.818	12	-24.7	8.25	1.18
	4.708	24	-20.5	2.72	0.609
Epidural-20 mm	2.8	6	-20	112.9	1.03
	4.702	30	-20.4	2.59	0.497
Subdural- 5 mm	2.812	6	-26.3	6.69	0.923
	4.726	6	-19.3	1.51	0.349
Subdural-10 mm	2.806	0.1	-26.8	6.21	1.22
	4.701	30.1	-20.1	2.27	0.769
Subdural-20 mm	2.824	18	-24.7	8.25	1.02
	4.708	24	-20.8	3.02	0.409
Subarachnoid-location 1	2.81	4	-31.4	1.62	1.2
	4.726	6	-17.7	0.05	0.624
Subarachnoid-location 2	2.806	0.2	-32.4	0.63	0.93
	4.72	12	-17.8	0.02	0.33
intracerebral	2.812	6	-33.8	0.84	0.939
	4.75	18	-18.1	0.27	0.344
Primary Intraventricular	2.812	6	-34.2	1.22	0.938
	4.750	18.4	-18.1	0.32	0.339
Secondary Intraventricular	2.812	6	-33.7	0.7	0.94
	4.75	18	-18.2	0.42	0.349

7. Analyzing and comparing results

Table 5 shows the effectiveness of the proposed antenna and its degree of discrimination between five different types of hemorrhagic strokes, in addition to discrimination within one type based on the change in its size over time, which represents an opportunity for the paramedic to determine the type of treatment with great accuracy. The first and second experiments were conducted on three different sizes of epidural and subdural hemorrhage (5, 10, 20) mm as shown in Figures 7 and 8, while the third and fourth experiments were conducted on two different locations of subarachnoid and intracerebral hemorrhage with a size of 20 mm as shown in Figures 9 and 10, while in the fifth experiment, primary and secondary intraventricular hemorrhage with a size of 20 mm were taken as shown in Figure 10. Through the above-mentioned results, we note the efficiency of the antenna in distinguishing between all cases, as well as discrimination within the same case with different sizes according to the shift in operating frequency and S11, as well as the change in the value of the specific absorption rate.

The comparison with previous works is shown in Table 6, and the contribution of our work lies in clarifying the location and type of hemorrhagic stroke. As far as we know, the types and locations have not been addressed accurately before. In addition, when comparing, we notice that the dimensions of the proposed antenna are smaller and the bandwidth is wider than all previous works. In addition, the safety of the antenna, despite its smaller size, is average among them.

Table 6. Comparison of the proposed antenna in this work and previous works.

Ref.	No. of Ant.	Dim. (mm^3)	B.W (GHz)	f_r (GHz)	SAR (W/kg)
(Salleh et al., 2019)	9	60×50×1.5	0.55	2.06 – 2.61	-
(Smida & Smida, 2020)	7	66×66 and 40×66	-	2.45	1.44x 10^{-5}
(Naghavi et al., 2023)	16	25×25×2	3.3	-	0.5
(Anwar et al., 2024)	2	27×18×1.6	2	1.9	1.25
	2	17×14×1.6	1	2.6	1.15
	2	90×40×1.6	1.5	2.6	0.506
	2	100×30×1.6	0.1	1.75	0.61
	2	27×18×1.6	1	2.4	0.85
(Singh et al., 2024)	2	66×66×0.8	1.67	2.45	0.0312
This work	1	30×35×0.6	3.196	2.806 4.732	0.894 0.319

8. Conclusions

An antenna with a Moroccan ornamental shape was proposed and designed to detect and recognize the five types of hemorrhagic stroke. It operates within the UWB range at a frequency of less than 3 GHz, capable of penetrating the middle of the white and gray cortex, thus speeding up treatment and reducing brain damage. In this work, the location of the stroke was chosen according to the type of stroke as mentioned in real medical references, in addition to mentioning the changes and damage that occur in the brain with each type, which was not addressed before. Different sizes of stroke were also examined, and the results showed the extent of the effect of changing the size and location on the sensitivity of the antenna and its efficiency. The small size of the antenna makes it easy to wear or install in ambulances or in the hands of paramedics to place it near the patient. It is also lightweight, highly accurate, and safe. Tests were conducted to evaluate its efficiency, in addition to measuring the directionality, gain, VSWR, FBR, and radiation pattern. The results were good in terms of detecting the stroke and determining its type, despite the small size of the antenna in comparison with previous works.

Conflict of interest

The authors have no conflict of interest to declare.

Acknowledgements

The authors would like to thank the College of Engineering, Mustansiriyah University, and the College of Engineering, University of Diyala for their support and assistance in accomplishing this work.

Funding

The authors received no specific funding for this work.

References

Abdul-Al, M., Amar, A. S., Elfergani, I., Littlehales, R., Ojaroudi Parchin, N., Al-Yasir, Y., ... & Abd-Alhameed, R. A. (2022). Wireless electromagnetic radiation assessment based on the Specific Absorption Rate (SAR): A review case study. *Electronics*, *11*(4), 511. https://doi.org/10.3390/electronics11040511

Alon, L., & Dehkharghani, S. (2021). A stroke detection and discrimination framework using broadband microwave scattering on stochastic models with deep learning. *Scientific Reports*, *11*(1). https://doi.org/10.1038/s41598-021-03043-y

Alqadami, A., Zamani, A., Trakic, A., & Abbosh, A. (2021). Flexible Electromagnetic Cap for Three-Dimensional Electromagnetic Head Imaging. *IEEE Transactions on Biomedical Engineering*, *68*(9). https://doi.org/10.1109/TBME.2021.3084313

Anwar, U., Arslan, T., & Lomax, P. (2024). Crescent Antennas as Sensors: Case of Sensing Brain Pathology. *Sensors*, *24*(4). https://doi.org/10.3390/s24041305

Dreier, J. P., Lemale, C. L., Horst, V., Major, S., Kola, V., Schoknecht, K., Scheel, M., Hartings, J. A., Vajkoczy, P., Wolf, S., Woitzik, J., & Hecht, N. (2024). Similarities in the Electrographic Patterns of Delayed Cerebral Infarction and Brain Death After Aneurysmal and Traumatic Subarachnoid Hemorrhage. *Translational Stroke Research*. https://doi.org/10.1007/s12975-024-01237-w

Essibayi, M. A., Ibrahim Abdallah, O., Mortezaei, A., Zaidi, S. E., Vaishnav, D., Cherian, J., Gungin, P., Altschul, D., & Labib, M. (2023). Natural History, Pathophysiology, and Recent Management Modalities of Intraventricular Hemorrhage. In *Journal of Intensive Care Medicine*. https://doi.org/10.1177/08850666231204582

Geoghegan, A. R., Shouldice, M., Mireskandari, K., & Smith, J. N. (2023). Subdural hemorrhages and severe retinal hemorrhages in a short fall with a rotational component. *Journal of AAPOS*, *27*(4). https://doi.org/10.1016/j.jaapos.2023.04.011

https://itis.swiss/virtual-population/tissue-properties/database/database-summary/.(n.d.).

I. Karunarathna, S. Bandara, A. Jayawardana, K. De Alvis, P. Gunasena, & U. T Ekanayake. (2024). *Comprehensive Management and Prognostic Considerations in Spontaneous Intracerebral Hemorrhage: A Clinical Review*.

IsHak, W. W. (Ed.). (2023). *Atlas of Psychiatry*. Springer International Publishing. https://doi.org/10.1007/978-3-031-15401-0

Lalitha, K., & Manjula, J. (2024). Experimental Verification of Microwave Head Imaging System Using Phantoms Fabricated from Artificial Tissue-Mimicking Materials. *Journal of Electronic Materials*, *53*(1), 129-140. https://doi.org/10.1007/s11664-023-10756-5

Liu, J., Chen, L., Xiong, H., & Han, Y. (2023). Review of microwave imaging algorithms for stroke detection. *Medical & Biological Engineering & Computing*, *61*(10), 2497–2510. https://doi.org/10.1007/s11517-023-02848-5

Naghavi, A. H., Hassani, H. R., & Oloumi, D. (2023). Improving the Probability of Stroke Detection inside the Human Head Using Wideband Polarimetric Synthetic Aperture Radar Imaging. *International Journal of RF and Microwave Computer-Aided Engineering*, *2023*. https://doi.org/10.1155/2023/5644220

Phan, A. C., Vo, V. Q., & Phan, T. C. (2018). Automatic Detection and Classification of Brain Hemorrhages. *Lecture Notes in Computer Science (Including Subseries Lecture Notes in Artificial Intelligence and Lecture Notes in Bioinformatics)*, *10752 LNAI*. https://doi.org/10.1007/978-3-319-75420-8_40

Salleh, A., Yang, C. C., Singh, M. S. J., & Islam, M. T. (2019). Development of antipodal Vivaldi antenna for microwave brain stroke imaging system. *Int. J. Eng. Technol*, *8*(3), 162-168.

Samsuzzaman, M., Siam Talukder, M., Alqahtani, A., Alharbi, A. G., Azim, R., Soliman, M. S., & Tariqul Islam, M. (2023). Circular slotted patch with defected grounded monopole patch antenna for microwave-based head imaging applications. *Alexandria Engineering Journal*, *65*, 41–57. https://doi.org/10.1016/j.aej.2022.10.034

Singh, A., Mandal, B., Biswas, B., Chatterjee, S., Banerjee, S., Mitra, D., & Augustine, R. (2024). Microwave Antenna-Assisted Machine Learning: A Paradigm Shift in Non-Invasive Brain Hemorrhage Detection. *IEEE Access*, *12*. https://doi.org/10.1109/ACCESS.2024.3371886

Smida, A., & Smida, A. (2020). Simulation and Analysis of Variable Antenna Designs for Effective Stroke Detection. *International Journal of Advanced Computer Science and Applications*, *11*(12). https://doi.org/10.14569/IJACSA.2020.0111230

Sohani, B., Tiberi, G., Ghavami, N., Ghavami, M., Dudley, S., & Rahmani, A. (2019). Microwave imaging for stroke detection: Validation on head-mimicking phantom. In *2019 PhotonIcs & Electromagnetics Research Symposium-Spring (PIERS-Spring)* (pp. 940-948). IEEE.

Tobon Vasquez, J. A., Rodriguez-Duarte, D. O., Origlia, C., Turvani, G., Scapaticci, R., Casu, M. R., Crocco, L., & Vipiana, F. (2022). Microwave Imaging Device Prototype for Brain Stroke 3D Monitoring. *2022 International Workshop on Antenna Technology (IWAT)*, 200–202. https://doi.org/10.1109/iWAT54881.2022.9810905

Zohor, A., Maliawan, S., Niryana, I. W., & Wardhana, W. (2024). Characteristics of Patients with Epidural Hemorrhage in Head Injury at a RSUP Prof. Dr. I.G.N.G Ngoerah in 2022. *Neurologico Spinale Medico Chirurgico*, *7*(1), 17–22. https://doi.org/10.4103/nsmc.nsmc_30_23